

LoLaFL: Low-Latency Federated Learning via Forward-only Propagation

Jierui Zhang, *Graduate Student Member, IEEE*, Jianhao Huang, *Member, IEEE*, and Kaibin Huang, *Fellow, IEEE*

Abstract—Federated learning (FL) has emerged as a widely adopted paradigm for enabling edge learning with distributed data while ensuring data privacy. However, the traditional FL with deep neural networks trained via backpropagation can hardly meet the low-latency learning requirements in the sixth generation (6G) mobile networks. This challenge mainly arises from the high-dimensional model parameters to be transmitted and the numerous rounds of communication required for convergence due to the inherent randomness of the training process. To address this issue, we adopt the state-of-the-art principle of maximal coding rate reduction to learn linear discriminative features and extend the resultant white-box neural network into FL, yielding the novel framework of Low-Latency Federated Learning (LoLaFL) via forward-only propagation. LoLaFL enables layer-wise transmissions and aggregation with significantly fewer communication rounds, thereby considerably reducing latency. Additionally, we propose two *nonlinear* aggregation schemes for LoLaFL. The first scheme is based on the proof that the optimal NN parameter aggregation in LoLaFL should be harmonic-mean-like. The second scheme further exploits the low-rank structures of the features and transmits the low-rank-approximated covariance matrices of features to achieve additional latency reduction. Theoretical analysis and experiments are conducted to evaluate the performance of LoLaFL. In comparison with traditional FL, the two nonlinear aggregation schemes for LoLaFL can achieve reductions in latency of over 91% and 98%, respectively, while maintaining comparable accuracies.

Index Terms—Low-latency learning, federated learning (FL), white-box neural network, forward-only propagation.

I. INTRODUCTION

With the growing volume of data and the increasing number of edge devices, the sixth generation (6G) mobile networks are envisioned to support a wide range of AI-based applications at the network edge, including augmented/mixed/virtual reality, connected robotics and autonomous systems, and smart cities and homes, among others [1], [2]. To realize this vision, researchers have been motivated to develop technologies to deploy AI models at the network edge. These technologies, collectively called edge learning, leverage the mobile-edge-computing platform to train edge-AI models among edge servers and devices [3], [4]. For its preservation of data privacy, federated learning (FL) emerges as a widely adopted solution for distributed edge learning, where local models are trained using local devices' data and sent to the server for updating the global model [5]–[8]. This collaborative training approach enables multiple devices and a server to train a global

model without sharing raw data. However, FL faces its own challenges. First, in scenarios where edge devices exhibit high mobility (e.g., autonomous cars and drones), they may move out of the range of an edge server before the learning process is completed. Second, in contexts with dynamic environments and evolving user behaviors, timely model retraining is crucial. These challenges necessitate the development of low-latency FL techniques to achieve faster response times [9]–[12].

However, achieving low-latency FL is challenging due to limited communication resources, which hinder the wireless exchange of high-dimensional stochastic gradients or models between devices and edge servers [13], [14]. Researchers have explored various approaches to allocate network resources and schedule participating devices such as wireless power transfer [15], resource allocation [16]–[19], and client scheduling [20], [21], to improve task performance. For example, in [21], a problem of joint learning, resource allocation, and user selection for FL over wireless networks was formulated and solved, improving the inference accuracy. Besides, the popular over-the-air computation (AirComp) technology is widely adopted to leverage the property of waveform superposition over a multi-access channel to realize simultaneous model uploading and over-the-air aggregation, thereby accelerating FL [22]–[24].

Despite these efforts to optimize the resource allocation for latency reduction, the bottleneck of low-latency FL lies in the high-dimensional gradients or model parameters to be transmitted and the numerous rounds for convergence [25]–[27]. For the first problem, approaches are considered to reduce the number of parameters to be transmitted. For example, model splitting introduces a method where the global model can be partitioned and distributed between server and devices for collaborative training, thereby reducing latency by transmitting only a portion of the gradients [28], [29]. Some lossy compression techniques can also be utilized. In particular, sparsification helps to drop insignificant model parameters [30], and quantization enables the use of fewer bits to represent an element for transmission [31]. For the second problem, techniques like federated transfer learning can be utilized for model initialization and speed up the convergence [32]. In essence, these two problems arise from the fundamental nature of deep neural networks (DNNs), such as Convolutional Neural Networks (CNNs) [33]. Specifically, their architectures are typically designed using a heuristic approach, and the training process involves random initialization and multiple rounds of weight updates via backpropagation (BP). This design principle, training method, and numerous

J. Zhang, J. Huang, and K. Huang are with the Department of Electrical and Electronic Engineering, The University of Hong Kong, Hong Kong. Emails: jrzhang@eee.hku.hk, jianhaoh@hku.hk, and huangk@eee.hku.hk (Corresponding author: J. Huang and K. Huang).

heuristic techniques involved in DNNs, collectively earn them the label of *black-box* [34]–[38]. The bottleneck cannot be easily overcome without challenging the current paradigm of FL, which necessitates the adoption of novel NN architectures and training approaches along with the design of a compatible FL framework.

Recently, the new approach of *white-box* has emerged, which focuses on providing rigorous mathematical principles to understand the underlying mechanisms of both the architecture and parameters of DNNs [39]. One notable example is the recent work in [40], which proposes a *forward-only* algorithm to directly construct an AI model from the intrinsic structures of data, without the need for multiple rounds of BP. Taking the classification task as an example, many real-world datasets exhibit specific structures and distributions in high-dimensional spaces. Then the objective for white-box DNNs is to learn the intrinsic structures underlying the data, namely the linear discriminative features in order to achieve effective classification [39], [40]. The principle of maximal coding rate reduction (MCR²) was proposed in [41], [42] to obtain these kinds of features from data. Therein, the so-called coding rate was introduced to quantify the volume of feature space spanned by the features up to a specific precision [43], as inspired by the classic rate-distortion theory [44]. MCR² calls for maximizing the volume of the entire feature space while minimizing that of the summed feature sub-spaces, which can be achieved through step-by-step feature transformation; the gradient information from each step forms the layer parameters of a novel *white-box neural network* constructed in a *forward-only* manner [40]. More surprisingly, it has been demonstrated that the white-box neural network has a similar architecture and comparable task accuracy to its black-box counterpart (e.g., the well-known ResNet [45]).

These white-box neural networks have two distinct characteristics. First, their parameters can be calculated from features directly and deterministically using formulae, eliminating the need of BP to update parameters. Second, such a model is constructed *only forwardly*, with each layer obtained based on the information from the previous layer. We advocate the design of low-latency FL by adopting the new training approach of white-box neural network to leverage its above characteristics. The first characteristic facilitates rapid convergence in model training. On the other hand, the second characteristic presents a new opportunity to advance low-latency FL: in each communication round, only the parameters of the latest layer instead of the whole model need to be transmitted. However, how to apply this white-box approach to FL in order to achieve low-latency edge learning remains an open problem. Solving it requires designing unique and compatible techniques for parameter transmissions and aggregation.

To this end, this paper presents a novel *low-latency federated learning* (LoLaFL) framework via forward-only propagation. LoLaFL features layer-wise transmissions and aggregation with much fewer communication rounds than traditional FL, thereby reducing communication latency dramatically. Specifically, in each communication round, only the latest

layer targeted for updating in the round, rather than the entire NN, is uploaded for aggregation and subsequently updated with the received aggregated one. The key differences between LoLaFL and traditional FL are summarized in Table I. The key contributions and findings of this paper are summarized as follows.

- **LoLaFL Framework:** The proposed framework consists of multi-round operations with the number of rounds determined by the number of model layers. In each round, the local parameters are calculated at edge devices based on local features and subsequently uploaded for aggregation at the edge server. The aggregated global parameters are then broadcast and used for local layer construction and local feature transformation. Unlike traditional FL, which requires the transmission of the entire model for updates at each communication round, LoLaFL only computes and transmits one layer of the neural network. This not only achieves low latency but also alleviates resource-constrained devices’ computation load.
- **Nonlinear Aggregation:** We have proved that the optimal aggregation for the global parameters of the white-box NN is not the traditional arithmetic mean (see e.g., FedAvg [5]) but the harmonic mean (HM) of the local parameters. Motivated by the finding, we propose two nonlinear aggregation schemes for LoLaFL, which are more flexible and powerful in capturing the complex relationships between the local and global parameters. Furthermore, we devise a scheme for compressing uploaded parameters by leveraging the low-rank structures of features. Incorporating this scheme to enhance the HM-like aggregation results in further reduction on latency.
- **Performance Analysis:** First, the communication latency and computational complexity are derived theoretically, which are demonstrated to be primarily determined by the dataset. Specifically, the latency and complexity are found to be proportional to the square and cube of data’s dimensionality, respectively, and both are proportional to the number of classes in the dataset. In contrast, the latency and complexity of traditional FL are primarily determined by the number of parameters and layers, with their effects being more significant when both the data dimensionality and the class number are small. Therefore, we conclude that LoLaFL exhibits smaller latency and complexity than traditional FL when both the data dimensionality and the class number are small. Next, we mathematically prove that the features or raw data cannot be recovered from the transmitted parameters, ensuring that LoLaFL is privacy-preserving.
- **Experiments:** The experiments are conducted in various scenarios to examine the performance of LoLaFL. By benchmarking against traditional FL, the results reveal that our two schemes for LoLaFL can achieve more than 91% and 98% reductions in latency, respectively, while maintaining comparable accuracies. The conver-

TABLE I: Comparison between LoLaFL and Traditional FL

Framework	Characteristics					
	Nature	Training	Target	What to transmit	Aggregation	Latency
Traditional FL	Black-box	Backpropagation	Minimized loss	Entire model	Linear	High
LoLaFL	White-box	Forward-only	Discriminative features	Single layer	Nonlinear	Low

gence speed of LoLaFL is ten times faster than traditional FL in terms of communication round. Additionally, LoLaFL demonstrates greater robustness with non-IID data.

The remainder of this paper is organized as follows. Section II compares the principles of black-box and white-box neural networks. The system model is introduced in Section III. The LoLaFL framework and two novel nonlinear aggregation schemes for it are presented in Section IV. In Section V, the communication latency and computational complexity are analyzed and the privacy guarantee of LoLaFL is characterized. Experimental results are provided in Section VI, followed by concluding remarks in Section VII.

II. PRINCIPLE COMPARISONS: BLACK-BOX VERSUS WHITE-BOX

A. Black-box DNNs via BP

DNNs can be seen as a nonlinear function that maps inputs to their corresponding outputs. In practice, the common approach is to design a heuristic architecture, and choose a loss function to measure the discrepancy between the network outputs and expected outputs for a specific learning task. The process to minimize the loss function, known as training, typically involves initializing the network parameters and then updating them via BP [34]. For classification, the global loss function is given by

$$F(\mathbf{w}) = \frac{1}{|\mathcal{D}|} \sum_{(\mathbf{x}_i, y_i) \in \mathcal{D}} f(\mathbf{w}, \mathbf{x}_i, y_i), \quad (1)$$

where \mathcal{D} is the dataset, and $f(\mathbf{w}, \mathbf{x}, y)$ is the cross entropy (CE) to measure the sample-wise error over the model, \mathbf{w} , w.r.t. sample \mathbf{x} and its true class, y [46]. Then, the SGD can be used to minimize the global loss function as follows

$$\mathbf{w}(\ell + 1) = \mathbf{w}(\ell) - \eta \frac{\partial F(\mathbf{w})}{\partial \mathbf{w}} \Big|_{\mathbf{w}=\mathbf{w}(\ell)}, \quad (2)$$

where η is the learning rate and $\mathbf{w}(\ell)$ is the model in training round ℓ . Despite their impressive performance in implementing various learning tasks, DNNs have long been regarded as black-boxes [34], [38]. It is challenging to interpret how the data is transformed as it passes through the DNNs and what the underlying mechanisms are.

FL has been adopted to deal with data privacy concerns associated with training the black-box DNNs at the edge. Instead of uploading the original dataset directly, FL focuses on transmitting model updates to renew the global model through multiple rounds of communication [12]. Specifically, in round $\ell \in \mathcal{L} = \{1, 2, \dots, L\}$, the edge server broadcasts the global model, $\mathbf{w}(\ell)$, to edge devices. Let $F_k(\mathbf{w})$ be the

local loss function over a local dataset, \mathcal{D}_k , (assuming uniform sizes) at device $k \in \mathcal{K} = \{1, 2, \dots, K\}$. Each device k calculates the gradient of the $F_k(\mathbf{w})$ w.r.t. $\mathbf{w}(\ell)$ based on \mathcal{D}_k , and the local model is updated as¹

$$\mathbf{w}_k(\ell + 1) = \mathbf{w}_k(\ell) - \eta \frac{\partial F_k(\mathbf{w})}{\partial \mathbf{w}} \Big|_{\mathbf{w}=\mathbf{w}(\ell)}. \quad (3)$$

Subsequently, each edge device uploads the updated model $\mathbf{w}_k(\ell + 1)$ to the edge server, and the edge server aggregates the models using the arithmetic mean as

$$\mathbf{w}(\ell + 1) = \frac{1}{K} \sum_{k=1}^K \mathbf{w}_k(\ell + 1). \quad (4)$$

The procedures of (3)-(4) are iteratively repeated until convergence or the maximal round number L is reached. However, significant communication latency is incurred for two reasons. First, the entire model needs to be transmitted by every device in each communication round. Second, numerous rounds are generally required to achieve convergence, due to the randomness in parameter initialization and SGD.

B. White-box NNs via Forward-only Propagation

The training of DNNs has been believed to follow the *parsimony* principle, whose goal is to learn a mapping $\phi(\cdot, \theta_1)$ with parameters θ_1 to transform data \mathbf{x} to a more compact and structured feature \mathbf{z} , facilitating downstream tasks [39]. Taking classification as an example, after the feature \mathbf{z} is obtained, a classifier $\psi(\cdot, \theta_2)$ with parameters θ_2 (see, e.g., [45]) is then used to predict its class y [40]. The entire pipeline is given as $\mathbf{x} \xrightarrow{\phi(\cdot, \theta_1)} \mathbf{z} \xrightarrow{\psi(\cdot, \theta_2)} y$. However, the mapping, $\phi(\cdot, \theta_1)$, and the classifier, $\psi(\cdot, \theta_2)$, are jointly optimized in black-box learning, without considering the features' distribution and characteristics. In contrast, white-box learning aims to find a mapping, $\phi(\cdot, \theta_1)$, that produces \mathbf{Z} with the following linear discriminative properties. Features \mathbf{Z} belonging to different classes exhibit low correlation, indicating that they occupy distinct sub-spaces (ideally orthogonal) and collectively span a large feature space. Conversely, features \mathbf{Z}^j from the same class $j \in \mathcal{J} = \{1, 2, \dots, J\}$ exhibit high correlation and span a small feature sub-space [40], [41]. This necessitates addressing three issues: 1) measuring the volume of the feature space, 2) finding the mapping $\phi(\cdot, \theta_1)$ to transform the data into linear discriminative features, and 3) designing a classifier to classify unlabeled samples. The details of the solutions are described as follows.

¹For ease of exposition, here we narrate FedSGD, a special case of FedAvg. It is assumed that in each round, there is only one epoch of training for each client model, and the full local dataset is treated as a mini-batch [5].

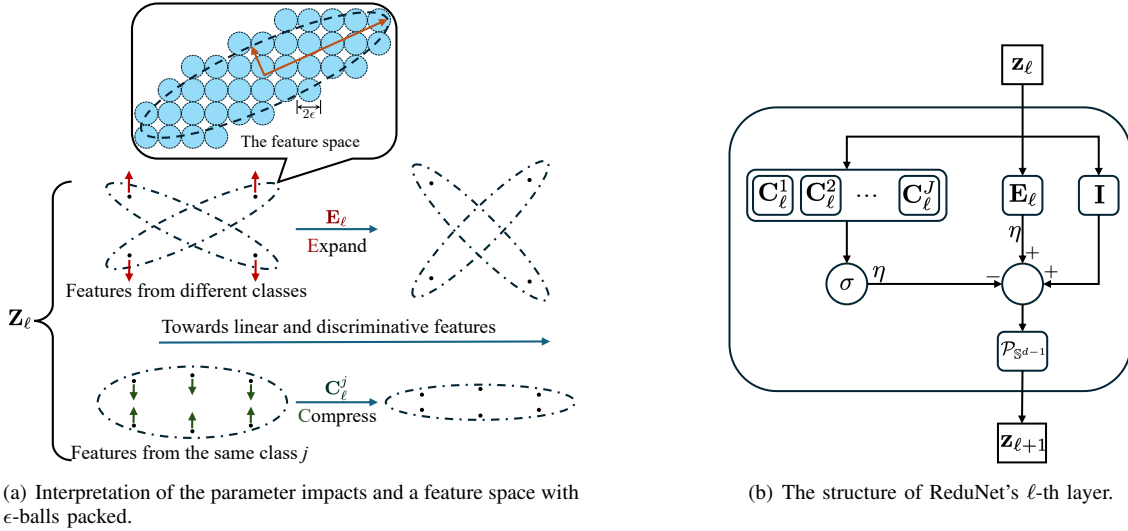


Fig. 1: Illustration of the ReduNet with forward-only propagation.

1) *Measuring the Feature Space with Coding Rate*: The *rate-distortion* was introduced in [44] to measure the compactness of a random distribution, defined as the minimal binary bits to encode a random variable up to a specific distortion. Fig. 1(a) illustrates a feature space packed with small balls with diameter 2ϵ , where the ball number represents the rate-distortion up to distortion ϵ . With unknown distribution and limited samples, computing the rate-distortion is typically intractable. Fortunately, distributions with linear discriminative properties allow closed-form expressions for the total bits to encode the samples [43]. With enough samples, the average coding length per sample, a.k.a. the *coding rate*, can approximate the rate-distortion, serving as a natural measure of a feature space's volume.

In particular, given data $\mathbf{X} = [\mathbf{x}^{(1)}, \mathbf{x}^{(2)}, \dots, \mathbf{x}^{(m)}] \in \mathbb{R}^{d \times m}$ with m samples and d dimensions, and their latent features $\mathbf{Z} = [\mathbf{z}^{(1)}, \mathbf{z}^{(2)}, \dots, \mathbf{z}^{(m)}]$ with the same shape, the coding rate of features \mathbf{Z} is

$$R(\mathbf{Z}, \epsilon) \triangleq \frac{1}{2} \log \det (\mathbf{I} + \alpha \mathbf{Z} \mathbf{Z}^*), \quad (5)$$

w.r.t. a certain distortion ϵ , where $(\cdot)^*$ denotes the transpose of a matrix or vector and $\alpha = d/(m\epsilon^2)$ [40], [43]. Similarly, the coding rate of the union of feature sub-spaces belonging to different classes is given by

$$R_c(\mathbf{Z}, \epsilon | \mathbf{\Pi}) \triangleq \sum_{j=1}^J \frac{\gamma^j}{2} \log \det (\mathbf{I} + \alpha^j \mathbf{Z} \mathbf{\Pi}^j \mathbf{Z}^*), \quad (6)$$

where $\alpha^j = d/(\text{tr}(\mathbf{\Pi}^j)\epsilon^2)$, $\gamma^j = \text{tr}(\mathbf{\Pi}^j)/m$. And $\mathbf{\Pi} \triangleq \{\mathbf{\Pi}^j \in \mathbb{R}^{m \times m}\}_{j=1}^J$ is a set of diagonal membership matrices to characterize the associated classes of data samples. For example, if sample i belongs to class j , then $\mathbf{\Pi}^j(i, i) = 1$, otherwise, $\mathbf{\Pi}^j(i, i) = 0$.

2) *Constructing ReduNet via MCR²*: With (5) and (6), the *coding rate reduction* can be defined as

$$\Delta R(\mathbf{Z}, \epsilon | \mathbf{\Pi}) \triangleq R(\mathbf{Z}, \epsilon) - R_c(\mathbf{Z}, \epsilon | \mathbf{\Pi}). \quad (7)$$

The linear discriminative properties call for a large volume of the whole feature space, $R(\mathbf{Z}, \epsilon)$, and a small volume of the individual feature spaces, $R_c(\mathbf{Z}, \epsilon | \mathbf{\Pi})$, which necessities maximizing $\Delta R(\mathbf{Z}, \epsilon | \mathbf{\Pi})$ w.r.t. normalized features \mathbf{Z} . Meanwhile, a mapping $\phi(\cdot, \theta_1)$ is needed to transform original data \mathbf{X} to features $\mathbf{Z}(\theta_1) = \phi(\mathbf{X}, \theta_1)$. This is called maximal coding rate reduction (MCR²), formulated as: $\max_{\theta_1} \Delta R(\mathbf{Z}, \epsilon | \mathbf{\Pi})$, s.t. $\|\mathbf{Z}^j(\theta_1)\|_F^2 = \text{tr}(\mathbf{\Pi}^j)$. The projected gradient ascent scheme [40] works for it:

$$\mathbf{Z}_{\ell+1} = \mathcal{P}_{\mathbb{S}^{d-1}}(\mathbf{Z}_{\ell} + \eta \frac{\partial \Delta R}{\partial \mathbf{Z}} |_{\mathbf{z}=\mathbf{z}_{\ell}}), \quad \ell = 1, 2, \dots, L, \quad (8)$$

where η is the learning rate, L is the number of transformations, \mathbf{Z}_{ℓ} are the features after $(\ell - 1)$ transformations, and $\mathcal{P}_{\mathbb{S}^{d-1}}(\cdot)$ denotes the projection operation which projects vectors to the unit sphere \mathbb{S}^{d-1} for normalization. Specifically, $\mathbf{Z}_1 = \mathcal{P}_{\mathbb{S}^{d-1}}(\mathbf{X}) \in \mathbb{R}^{d \times m}$.

To better understand the gradient, with (5)-(7), the gradient in (8) is calculated as

$$\begin{aligned} & \frac{\partial \Delta R}{\partial \mathbf{Z}} |_{\mathbf{z}=\mathbf{z}_{\ell}} \\ &= \underbrace{\alpha(\mathbf{I} + \alpha \mathbf{Z}_{\ell} \mathbf{Z}_{\ell}^*)^{-1}}_{\triangleq \mathbf{E}_{\ell}} \mathbf{Z}_{\ell} - \sum_{j=1}^J \gamma^j \underbrace{\alpha^j (\mathbf{I} + \alpha^j \mathbf{Z}_{\ell} \mathbf{\Pi}^j \mathbf{Z}_{\ell}^*)^{-1}}_{\triangleq \mathbf{C}_{\ell}^j} \mathbf{Z}_{\ell} \mathbf{\Pi}^j. \end{aligned} \quad (9)$$

The matrices \mathbf{E}_{ℓ} and \mathbf{C}_{ℓ}^j form the layer parameters of a neural network, called *ReduNet*, which is constructed via forward-only propagation. As \mathbf{E}_{ℓ} and \mathbf{C}_{ℓ}^j are from (5) and (6) respectively, \mathbf{E}_{ℓ} forces \mathbf{Z}_{ℓ} from different classes to diverge while \mathbf{C}_{ℓ}^j compresses \mathbf{Z}_{ℓ}^j from the same class j , as shown

in Fig. 1(a). Upon obtaining $\{\mathbf{E}_\ell\}_{\ell=1}^L$ and $\{\mathbf{C}_\ell^j\}_{j=1, \ell=1}^{J,L}$, the training is finished. Since \mathbf{E}_ℓ and \mathbf{C}_ℓ^j are derived from the rigorous mathematical principle of MCR² and their effects are fully interpretable, ReduNet earns the label of *white-box* [40].

3) *Employing ReduNet for Inference*: As for inference, considering an unlabeled sample \mathbf{x} and its transformed feature \mathbf{z}_ℓ in layer ℓ , the gradient is $(\mathbf{E}_\ell \mathbf{z}_\ell - \sum_{j=1}^J \gamma^j \mathbf{C}_\ell^j \boldsymbol{\pi}^j(\mathbf{z}_\ell))$, where $\boldsymbol{\pi}(\mathbf{z}_\ell)$ is the probability distribution vector of \mathbf{z}_ℓ . Building upon the insight from (9), gradient $-\mathbf{C}_\ell^j \mathbf{z}_\ell$ guides \mathbf{z}_ℓ towards the sub-space of its true class, which makes $\|\mathbf{C}_\ell^j \mathbf{z}_\ell\|$ small if \mathbf{z}_ℓ belongs to class j and large otherwise. This facilitates the estimation of $\boldsymbol{\pi}^j(\mathbf{z}_\ell)$ using softmax as

$$\hat{\boldsymbol{\pi}}^j(\mathbf{z}_\ell) \triangleq \sigma(\left(\|\mathbf{C}_\ell^1 \mathbf{z}_\ell\|, \|\mathbf{C}_\ell^2 \mathbf{z}_\ell\|, \dots, \|\mathbf{C}_\ell^J \mathbf{z}_\ell\|\right))^j \quad (10)$$

$$= \exp(-\lambda \|\mathbf{C}_\ell^j \mathbf{z}_\ell\|) / \sum_{j=1}^J \exp(-\lambda \|\mathbf{C}_\ell^j \mathbf{z}_\ell\|), \quad (11)$$

where λ is a hyperparameter. The structure of layer ℓ for transforming feature \mathbf{z}_ℓ to $\mathbf{z}_{\ell+1}$ is illustrated in Fig. 1(b). Then a classifier for ReduNet is given by $\hat{j} = \arg \max_{j \in \mathcal{J}} (\hat{\boldsymbol{\pi}}^j(\mathbf{z}_L))$.

As ReduNet is constructed layer by layer, a novel FL framework can be designed to enable layer-wise construction and update, as presented in the following sections.

III. SYSTEM MODEL

Consider a general FL system in which K edge devices with their local datasets aim to learn the optimal NN parameters as coordinated by the edge server over a total of L communication rounds. Similar to the traditional FL procedure, in each communication round, local models are updated based on local datasets, the updated parameters are uploaded to the edge server for aggregation, and the aggregated parameters are subsequently broadcast to edge devices for updating local models (elaborated in Section IV-A). The transmission process in each communication round is described as follows.

The orthogonal frequency-division multiple access (OFDMA) is adopted, where the available bandwidth B is divided into M orthogonal subchannels, and each edge device is assigned M/K sub-channels to avoid the interference [22], [47]. At edge device k , local parameters $\mathbf{g}_k \in \mathbb{R}^q$ are to be uploaded. Each parameter is quantized into Q bits by uniform quantization as in [24] which are then modulated into symbols. The i -th symbol received at the server is given by

$$y_{i,k} = h_k \sqrt{p_k} x_{i,k} + n_{i,k}, \quad (12)$$

where $x_{i,k}$ is the i -th symbol from edge device k , h_k is the channel coefficient between device k and server, p_k is the associated power control policy, and $n_{i,k} \sim \mathcal{CN}(0, \nu_n^2)$ is the independent and identically distributed (IID) additive white Gaussian noise (AWGN). We assume a slow fading channel where h_k remains constant over a single uploading round and is assumed to be known to both sides. We model h_k as Rayleigh fading with $h_k \sim \mathcal{CN}(0, 1)$, where the coefficients are IID across different devices and different rounds [19], [24].

In FL, model aggregation is implemented after all devices have completed uploading their local models. Consequently, poor channel conditions can impede the local model uploading process on some devices, thereby increasing overall latency. To mitigate fading, we adopt the truncated power control policy, as in [22]:

$$p_k = \begin{cases} \rho_0 / |h_k|^2, & |h_k|^2 \geq \tau, \\ 0, & |h_k|^2 < \tau, \end{cases} \quad (13)$$

where ρ_0 is a scaling factor to meet the power constraint in the sequel, and τ is the power cut-off threshold to avoid deep fading. The power constraint for each device is $\mathbb{E}[p_k] \leq P_0$, with P_0 being the power budget per device. By analyzing this expectation, we can derive the exact value of $\rho_0 = P_0 / \text{Ei}(\tau)$, where $\text{Ei}(x) = \int_x^\infty \frac{1}{s} \exp(-s) ds$ [48]. This policy can result in an outage probability of $\xi \triangleq \Pr(|h_k|^2 < \tau) = 1 - \exp(-\tau)$. According to above settings, when $|h_k|^2 \geq \tau$, the transmission rate of device k is given by

$$r_k = \frac{B}{K} \log_2 \left(1 + \frac{K P_0}{M \nu_n^2 \text{Ei}(\tau)} \right). \quad (14)$$

Then, the uploading communication latency (in seconds) for device k in round ℓ is given by

$$T_{\text{comm}, \ell, k} = \frac{K q Q}{B \log_2 \left(1 + \frac{K P_0}{M \nu_n^2 \text{Ei}(\tau)} \right)}. \quad (15)$$

For devices whose channels fail to meet the threshold τ , they give up transmission without repeated attempts. Thus, no additional retransmission latency is incurred. The resultant loss could degrade the learning performance, which will be investigated in experiments.

The edge server demodulates the received symbols to recover the bit streams and reconstruct the local parameters $\bar{\mathbf{g}}_k$ for calculating the global ones $\bar{\mathbf{g}}$. Subsequently, the global parameters are broadcast to devices to replace their local models. Since the edge server typically has higher transmit power and full downlink bandwidth availability, the broadcasting latency is negligible compared to that of uploading and is thus omitted from our analysis [16].

IV. LOLAFL VIA FORWARD-ONLY PROPAGATION

In this section, we propose a novel FL framework for achieving low-latency edge learning based on the white-box NN introduced in Section II-B. First, the model uploading and aggregation processes of the proposed framework based on the forward-only propagation algorithm are introduced. Then, two novel nonlinear aggregation methods are presented.

A. The LoLaFL Framework

We propose a novel LoLaFL framework as shown in Fig. 2. Unlike traditional FL where the whole model is exchanged between the edge devices and the server, LoLaFL enables the white-box NNs to be constructed and updated in a layer-wise manner. The details are provided as follows.

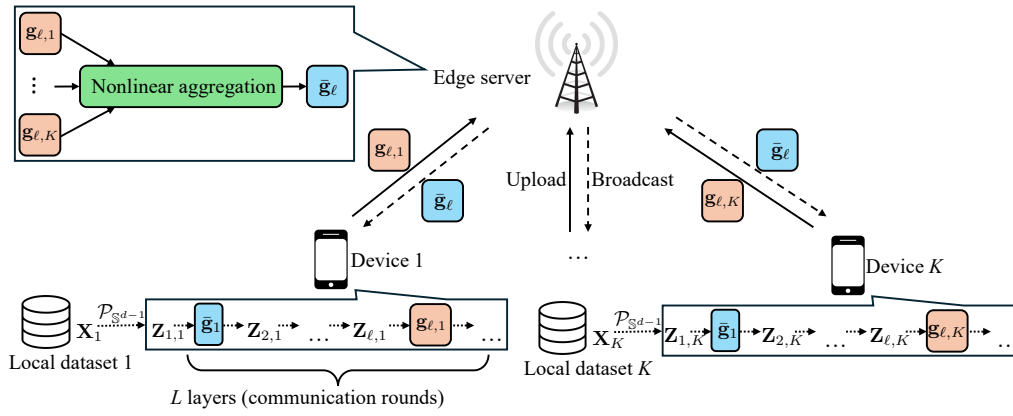


Fig. 2: The model updating and aggregation processes of LoLaFL.

1) *Layer-wise Construction*: This part corresponds to the local training in traditional FL, but the approach is fundamentally different. In each communication round in LoLaFL, the parameters of a single layer are calculated directly based on the latest features at each device. Initially, the local data samples at device k are normalized, outputting the features, i.e., $\mathbf{Z}_{1,k} = \mathcal{P}_{\mathcal{S}^{d-1}}(\mathbf{X}_k) \in \mathbb{R}^{d \times m_k}$, where m_k is the number of samples at device k , and their associated classes are characterized by the diagonal membership matrices, $\{\mathbf{\Pi}_k^j \in \mathbb{R}^{m_k \times m_k}\}_{j=1}^J$, as defined in (6). In communication round $\ell \in \mathcal{L} = \{1, 2, \dots, L\}$, the local feature samples, $\mathbf{Z}_{\ell,k}$, and their corresponding membership matrices, $\{\mathbf{\Pi}_k^j\}_{j=1}^J$, at edge device k are utilized to calculate the NN parameters according to (9). In other words,

$$\mathbf{E}_{\ell,k} \triangleq \alpha_k (\mathbf{I} + \alpha_k \mathbf{Z}_{\ell,k} \mathbf{Z}_{\ell,k}^*)^{-1}, \quad (16)$$

$$\mathbf{C}_{\ell,k}^j \triangleq \alpha_k^j (\mathbf{I} + \alpha_k^j \mathbf{Z}_{\ell,k} \mathbf{\Pi}_k^j \mathbf{Z}_{\ell,k}^*)^{-1}. \quad (17)$$

In the formulae, $\alpha_k = d/(m_k \epsilon^2)$, $\alpha_k^j = d/(\text{tr}(\mathbf{\Pi}_k^j) \epsilon^2)$, and $\gamma_k^j = \text{tr}(\mathbf{\Pi}_k^j)/m_k$ are the local coefficients. We assume that all edge devices and the edge server share the information of m and $\text{tr}(\mathbf{\Pi}^j)$, and have an identical setting of ϵ , which means all edge devices and the edge server can calculate the global coefficients α , α^j , and γ^j individually.

2) *Layer-wise Transmission and Aggregation*: Different from traditional FL that focuses on the whole model, LoLaFL only uploads and aggregates one model layer per round. Specifically, after the ℓ -th NN layer with parameters, $\mathbf{g}_{\ell,k}$, is constructed, device k aims to transmit this layer's parameters to the server for aggregation. Depending on the special white-box structures given in (16) and (17), the transmitted parameters can be either the exact NN parameters or the latent covariance matrices (CMs) of features. This calls for different aggregation designs, which will be introduced in the following subsections in detail. Here, we let the transmitted parameters be $\mathbf{g}_{\ell,k}$ to illustrate the LoLaFL framework as shown in Fig. 2. When the server receives $\{\mathbf{g}_{\ell,k}\}_{k=1}^K$, the global parameters $\bar{\mathbf{g}}_\ell$ are calculated and updated, which are then broadcast to edge devices. At edge device k , its local parameters, $\mathbf{g}_{\ell,k}$, is

replaced by the received global parameters $\bar{\mathbf{g}}_\ell$. Afterwards, the local features $\mathbf{Z}_{\ell,k}$ are input into the ℓ -th layer with parameters, $\bar{\mathbf{g}}_\ell$, to output $\mathbf{Z}_{\ell+1,k}$ for constructing the $(\ell + 1)$ -th layer. The LoLaFL algorithm is summarized in Algorithm 1.

B. Harmonic-mean-Like Aggregation

In this subsection, the parameters to be exchanged between edge devices and the edge server are the parameters of the white-box NN, i.e., $\mathbf{g}_{\ell,k} = \{\mathbf{E}_{\ell,k}\} \cup \{\mathbf{C}_{\ell,k}^j\}_{j=1}^J$. However, the FedAvg in traditional FL is not optimal for the aggregation in this scenario, because the NN parameters are derived from the features with nonlinear mappings. Hence, a novel compatible aggregation scheme is designed for LoLaFL as follows.

Referring to (16) and (17), the local NN parameters, $\{\mathbf{E}_{\ell,k}\} \cup \{\mathbf{C}_{\ell,k}^j\}_{j=1}^J$, are determined by the CMs of local features, i.e., $\mathbf{R}_{\ell,k} \triangleq \mathbf{Z}_{\ell,k} \mathbf{Z}_{\ell,k}^*$ and $\mathbf{R}_{\ell,k}^j \triangleq \mathbf{Z}_{\ell,k} \mathbf{\Pi}_k^j \mathbf{Z}_{\ell,k}^*$. And referring to (9), the global NN parameters, $\{\mathbf{E}_\ell\} \cup \{\mathbf{C}_\ell^j\}_{j=1}^J$, are determined by the CMs of global features, i.e., $\bar{\mathbf{R}}_\ell \triangleq \mathbf{Z}_\ell \mathbf{Z}_\ell^*$ and $\bar{\mathbf{R}}_\ell^j \triangleq \mathbf{Z}_\ell \mathbf{\Pi}^j \mathbf{Z}_\ell^*$. Therefore, aggregation of $\{\mathbf{E}_{\ell,k}\} \cup \{\mathbf{C}_{\ell,k}^j\}_{j=1}^J$ fundamentally requires aggregation of the CMs of local features. To this end, we obtain the following results.

Lemma 1 In each communication round ℓ , the CMs of global features can be decomposed as the summation of the CMs of local features. In other words,

$$\bar{\mathbf{R}}_\ell = \sum_{k=1}^K \mathbf{R}_{\ell,k} \quad \text{and} \quad \bar{\mathbf{R}}_\ell^j = \sum_{k=1}^K \mathbf{R}_{\ell,k}^j. \quad (18)$$

Proof: See Appendix A.

Proposition 1 (HM-like aggregation): In each communication round ℓ , the global NN parameters, $\bar{\mathbf{g}}_\ell = \{\mathbf{E}_\ell\} \cup \{\mathbf{C}_\ell^j\}_{j=1}^J$, can be calculated directly with local NN parameters, $\{\mathbf{g}_{\ell,k}\}_{k=1}^K$, as

$$\bar{\mathbf{E}}_\ell = \left(\sum_{k=1}^K (\mathbf{E}_{\ell,k})^{-1} \right)^{-1}, \quad (19)$$

$$\bar{\mathbf{C}}_\ell^j = \left(\sum_{k=1}^K (\mathbf{C}_{\ell,k}^j)^{-1} \right)^{-1}. \quad (20)$$

Algorithm 1 Proposed LoLaFL Algorithm

Input: $\{\mathbf{X}_k \in \mathbb{R}^{d \times m_k}\}_{k=1}^K$, $\{\mathbf{\Pi}_k^j \in \mathbb{R}^{m_k \times m_k}\}_{j=1, k=1}^{J, K}$, ϵ , λ , learning rate η , layer number L , channel inversion threshold τ (\cdot , SVD threshold β_0). *Initialization:* $\{\mathbf{Z}_{1,k} = \mathcal{P}_{\mathbb{S}^{d-1}}(\mathbf{X}_k) \in \mathbb{R}^{d \times m_k}\}_{k=1}^K$, $\alpha = d/(m\epsilon^2)$, $\{\alpha^j = d/(\text{tr}(\mathbf{\Pi}^j)\epsilon^2)\}_{j=1}^J$, $\{\gamma^j = \text{tr}(\mathbf{\Pi}^j)/m\}_{j=1}^J$.

- 1: **for** $\ell = 1$ to L **do**
- 2: **for** $k = 1$ to K **do**
- 3: Local NN parameter calculation ((16) and (17), for the HM-like scheme) or local SVD of covariance matrices calculation ((21a) and (21b), for the CM-based scheme).
- 4: **if** Deep fading ($|h_k|^2 < \tau$) **then**
- 5: Device k quits parameters uploading in this round.
- 6: **else**
- 7: Local NN parameters (for the HM-like scheme) or decomposed covariance matrices (for the CM-based scheme) uploading.
- 8: **end if**
- 9: **end for**
- 10: Aggregation with local NN parameters ((19) and (20), for the HM-like scheme), or with local covariance matrices ((22a) and (23b), for the CM-based scheme), for global ones.
- 11: (Global NN parameter calculation (9) for the CM-based scheme, if needed.)
- 12: Global NN parameters or decomposed covariance matrices broadcasting.
- 13: **for** $k = 1$ to K **do**
- 14: (NN parameter calculation (16), (17) for the CM-based scheme.)
- 15: Feature transformation (8).
- 16: **end for**
- 17: **end for**

Output: Learned parameters of $\{\mathbf{E}_\ell\}_{\ell=1}^L$ and $\{\mathbf{C}_\ell^j\}_{j=1, \ell=1}^{J, L}$.

Proof: See Appendix B.

The preceding results demonstrate how to calculate the global NN parameters from the local NN parameters in LoLaFL. Specifically, if we treat the matrices as numbers and the matrix inversion as reciprocal, these two formulae suggest that the global NN parameters are like the *harmonic mean* of the corresponding local NN parameters. In the ℓ -th communication round, the procedures are discussed as follows. Firstly, the local NN parameters, $\mathbf{E}_{\ell,k}$ and $\mathbf{C}_{\ell,k}^j$, are calculated with local features using (16) and (17). Then, the local NN parameters at each edge device are uploaded, and the edge server receives the local NN parameters as $(\bar{\mathbf{E}}_{\ell,k} = \mathbf{E}_{\ell,k} + \mathbf{N}_{\ell,k})$ and $(\bar{\mathbf{C}}_{\ell,k}^j = \mathbf{C}_{\ell,k}^j + \mathbf{N}_{\ell,k}^j)$, with the distortions, $\mathbf{N}_{\ell,k}$ and $\mathbf{N}_{\ell,k}^j$, specified in the system model. After uploading, the global NN parameters, $\bar{\mathbf{E}}_\ell$ and $\bar{\mathbf{C}}_\ell^j$, are calculated based on the received local NN parameters, using (19) and (20) by replacing $\mathbf{E}_{\ell,k}$ with $\bar{\mathbf{E}}_{\ell,k}$ and $\mathbf{C}_{\ell,k}^j$ with $\bar{\mathbf{C}}_{\ell,k}^j$. Subsequently, the global NN parameters $\bar{\mathbf{E}}_\ell$ and $\bar{\mathbf{C}}_\ell^j$ are broadcast to all devices. Finally,

each edge device updates its current layer, i.e., setting its current NN parameters as $\mathbf{E}_{\ell,k} = \bar{\mathbf{E}}_\ell$ and $\mathbf{C}_{\ell,k}^j = \bar{\mathbf{C}}_\ell^j$. They use the new NN parameters to transform the local features using (8), which prepares for updating the next layer in the following round.

C. Covariance-matrix-Based Aggregation

In this subsection, the parameters to be exchanged between edge devices and the edge server are the collection of the low-rank versions of local CMs, i.e., $\mathbf{g}_{\ell,k} = \{\tilde{\mathbf{R}}_{\ell,k}\} \cup \{\tilde{\mathbf{R}}_{\ell,k}^j\}_{j=1}^J$, the details of which are given in the sequel. We propose this approach because the NN parameters in the HM-like scheme have very high dimensionality and may be difficult to compress. In contrast, these CMs have low-rank structures, resulting from the low-rank structures of the features. This is because ReduNet is making features sparse, so the intrinsic dimensionality of the features is small, as shown in Fig. 1(a). Therefore, these CMs can be further compressed, which motivates the design of CM-based aggregation as follows. For ease of notation, in the following exposition, the index ℓ is omitted whenever no confusion arises.

The procedure of each communication round is described as follows. Firstly, the local CMs \mathbf{R}_k and \mathbf{R}_k^j at each edge device are calculated. Then, the local CMs at each edge device are decomposed with *singular value decomposition* (SVD) [49] and approximated to some degree as follows:

$$\mathbf{R}_k \approx \tilde{\mathbf{R}}_k = \sum_{i=1}^{s_k} \sigma_{i,k} \mathbf{u}_{i,k} \mathbf{v}_{i,k}^*, \quad (21a)$$

$$\mathbf{R}_k^j \approx \tilde{\mathbf{R}}_k^j = \sum_{i=1}^{s_k^j} \sigma_{i,k}^j \mathbf{u}_{i,k}^j \mathbf{v}_{i,k}^{j*}. \quad (21b)$$

In the preceding formulae, s_k and s_k^j are the minimal possible s to remain desired information: $\beta \triangleq \sum_{i=1}^s \sigma_i / \sum_{i=1}^d \sigma_i \geq \beta_0$, where β is the information remaining rate and β_0 is the threshold. We define the compression rate δ as the expected ratio of the number of chosen singular values to the total number of singular values. Then the singular values and vectors are uploaded as $\bar{\sigma}_{i,k} = \sigma_{i,k} + n_{i,k}$, $\bar{\mathbf{u}}_{i,k} = \mathbf{u}_{i,k} + \mathbf{n}_{\mathbf{u},i,k}$, $\bar{\mathbf{v}}_{i,k} = \mathbf{v}_{i,k} + \mathbf{n}_{\mathbf{v},i,k}$, $\bar{\sigma}_{i,k}^j = \sigma_{i,k}^j + n_{i,k}^j$, $\bar{\mathbf{u}}_{i,k}^j = \mathbf{u}_{i,k}^j + \mathbf{n}_{\mathbf{u},i,k}^j$, and $\bar{\mathbf{v}}_{i,k}^j = \mathbf{v}_{i,k}^j + \mathbf{n}_{\mathbf{v},i,k}^j$, where the distortions are specified in the system model. Thus the low-rank-approximated CMs can be reconstructed at the edge server as

$$\bar{\mathbf{R}}_k = \sum_{i=1}^{s_k} \bar{\sigma}_{i,k} \bar{\mathbf{u}}_{i,k} \bar{\mathbf{v}}_{i,k}^*, \quad (22a)$$

$$\bar{\mathbf{R}}_k^j = \sum_{i=1}^{s_k^j} \bar{\sigma}_{i,k}^j \bar{\mathbf{u}}_{i,k}^j \bar{\mathbf{v}}_{i,k}^{j*}. \quad (22b)$$

Then we can calculate the CMs of global features, $\bar{\mathbf{R}}$ and $\bar{\mathbf{R}}^j$, using (18) by replacing $\mathbf{R}_{\ell,k}$ with $\bar{\mathbf{R}}_{\ell,k}$ and $\mathbf{R}_{\ell,k}^j$ with $\bar{\mathbf{R}}_{\ell,k}^j$. If needed (when the edge server also needs the entire model), the global NN parameters can be calculated using (9)

by replacing $\mathbf{Z}_\ell \mathbf{Z}_\ell^*$ with $\bar{\mathbf{R}}$ and $\mathbf{Z}_\ell \mathbf{\Pi}^j \mathbf{Z}_\ell^*$ with $\bar{\mathbf{R}}^j$. Again, we can apply low-rank approximation to the global CMs as

$$\bar{\mathbf{R}} \approx \tilde{\mathbf{R}} = \sum_{i=1}^{s_0} \sigma_i \mathbf{u}_i \mathbf{v}_i^*, \quad (23a)$$

$$\bar{\mathbf{R}}^j \approx \tilde{\mathbf{R}}^j = \sum_{i=1}^{s_0^j} \sigma_i^j \mathbf{u}_i^j \mathbf{v}_i^{j*}. \quad (23b)$$

Subsequently, the singular values and singular vectors are broadcast to each edge device. The low-rank-approximated global CMs can be reconstructed at each edge device using (23a) and (23b). Finally, each edge device calculates the NN parameters using the definition provided in (9) by replacing $\mathbf{Z}_\ell \mathbf{Z}_\ell^*$ with $\bar{\mathbf{R}}$ and $\mathbf{Z}_\ell \mathbf{\Pi}^j \mathbf{Z}_\ell^*$ with $\bar{\mathbf{R}}^j$. The parameters are then utilized to transform the features according to (8), which prepares for updating the next layer in the following round.

V. PERFORMANCE ANALYSIS

In this section, we first analyze the communication latency and computational complexity of the LoLaFL with a comparison with traditional FL. Next, we provide a proof of the privacy guarantee in LoLaFL.

A. Latency Analysis

For brevity, we only consider the number of parameters uploaded from each device k , from which the communication latency can be easily obtained. For LoLaFL with HM-like aggregation, in each round, uploading of local parameters yields $(J+1)d^2$. So, the total number of parameters transmitted over L rounds is $L(J+1)d^2$. For LoLaFL with CM-based aggregation, since SVD is used to reduce the latency, in each round, the upload of compressed CMs yields $(J+1)(2\delta d^2 + \delta d)$. Thus, the total number of parameters transmitted over L rounds is $L(J+1)(2\delta d^2 + \delta d)$. For traditional FL, let W denote the parameter number of the utilized DNN model. In each round, uploading the local parameters yields W . And the total number of parameters transmitted over L rounds is LW .

As summarized in Table II, considering the number of parameters to be transmitted and focusing on the dominant part (i.e., terms with d^2) in the expressions, the CM-based scheme outperforms the HM-like scheme, as long as $\delta < 1/2$. The latency of LoLaFL is proportional to d^2 and J while that of traditional FL does not depend on d and J . This means that for datasets with high dimensionality and a large number of classes, LoLaFL may not outperform traditional FL.

B. Complexity Analysis

For computational complexity, we only consider matrix multiplication, matrix inversion, and SVD (if any), as these operations dominate the complexity. Generally, the multiplication of two matrices with shapes $(m \times n)$ and $(n \times k)$ takes mnk operations. For an invertible $n \times n$ matrix, the computational complexity of calculating its inversion is $O(n^3)$. For an $m \times n$ matrix, the computational complexity of calculating its SVD is $O(mn \min(m, n))$ [50].

For LoLaFL with HM-like aggregation, in each round, according to (16) and (17), the parameter calculation at edge devices requires $\sum_{k=1}^K O(2m_k d^2 + (J+1)d^3) = O((J+1)Kd^3 + 2md^2)$. Based on (19) and (20), the aggregation at edge server requires $O((J+1)(K+1)d^3)$. According to (8), feature transformation requires $\sum_{k=1}^K O((J+1)m_k d^2) = O((J+1)md^2)$. Combining these operations yields a computational complexity of $O((J+1)(2K+1)d^3 + (J+3)md^2)$.

For LoLaFL with CM-based aggregation, in each round, the local CM calculation at edge devices requires $\sum_{k=1}^K O(2m_k d^2) = O(2md^2)$. According to (21a) and (21b), the SVD for the local CMs requires $\sum_{k=1}^K O((J+1)d^3) = O((J+1)Kd^3)$. The reconstruction process at the edge server requires $\sum_{k=1}^K O(2\delta d^2) = O(2\delta Kd^2)$. The aggregation at the edge server can be omitted because only addition is used. According to (23a) and (23b), the SVD for the global CMs requires $O((J+1)d^3)$, and the reconstruction process at the edge devices requires $\sum_{k=1}^K O(2\delta d^2) = O(2\delta Kd^2)$. The parameter calculation and feature transformation require $O((J+1)Kd^3)$ and $\sum_{k=1}^K O((J+1)m_k d^2) = O((J+1)md^2)$ respectively. Combining these operations yields $O((J+1)(2K+1)d^3 + [4\delta K + (J+3)m]d^2)$.

For traditional FL, we analyze a fully-connected NN with N layers, each containing n nodes. During forward propagation, passing m_k samples from the input layer to the first hidden layer incurs $O(m_k dn)$. Passing them through the subsequent $(N-1)$ hidden layers yields $O((N-1)m_k n^2)$, and passing them from the last hidden layers to the output layer yields $O(m_k Jn)$. The low complexity associated with adding the bias term and calculating the activation function is omitted. Combining these components results in the complexity of forward propagation for device k as $O(m_k(dn + (N-1)n^2 + Jn))$, which is equivalent to that of the backpropagation. Therefore, the overall complexity of forward propagation and backpropagation in all edge devices is given by $\sum_{k=1}^K O(2m_k(dn + (N-1)n^2 + Jn)) = O(2m((N-1)n^2 + (J+d)n))$ [51].

As summarized in Table II, for LoLaFL, if we only focus on the dominant part (i.e., terms with d^3) in the expressions, the HM-like and CM-based schemes have comparable computational complexity. The computational complexity of LoLaFL is proportional to d^3 and J , while for traditional FL, the dominant part is proportional to n^2 and N . This indicates that the bottleneck of LoLaFL is primarily related to the complexity of the datasets, while that of traditional FL is associated with the width and depth of the neural network.

As demonstrated by the experiments in the sequel, the CM-based scheme achieves over 98% reduction in total latency (communication latency and computation latency) compared with traditional FL. The low latency results from the following three aspects:

- **Forward-only propagation:** In LoLaFL, the layers are constructed in a forward manner, and the parameters are calculated directly and deterministically according to formulae. Since these parameters of each layer in LoLaFL are near-optimal, once a layer is constructed, no

TABLE II: The Summary of Communication Latency (in parameter) and Computational Complexity

Metrics	Comparison of Different Schemes		
	LoLaFL (HM-like)	LoLaFL (CM-based)	Traditional FL
Latency (per device)	$L(J+1)d^2$	$L(J+1)(2\delta d^2 + \delta d)$	LW
Complexity (per round)	$O((J+1)(2K+1)d^3 + (J+3)md^2)$	$O((J+1)(2K+1)d^3 + [4\delta K + (J+3)m]d^2)$	$O(2m((N-1)n^2 + (J+d)n))$

BP is needed. In contrast, traditional FL requires random initialization and multiple rounds of BP to update the whole model. Therefore, we are comparing a layer in LoLaFL with the entire black-box model in traditional FL, in each communication round.

- **Novel aggregation scheme:** Unlike HM-like aggregation and FedAvg, the novel CM-based aggregation makes use of CMs. The low-rank structures of features allow for compression of the CMs, enabling the transmission of a smaller volume of data (singular vectors and singular values rather than CMs). This helps to further reduce the communication latency.
- **Minimal communication round:** In our experiments, it has been observed that merely a few rounds of communication can achieve comparable accuracy. The reasons are twofold: model size and normalization. 1) Generally, in deep learning, a larger model size means better performance. ResNet and ResNet have some similarities [40], and the parameter number of a single layer of ResNet (about 6.8×10^6 , near-optimal) is already comparable with the entire ResNet-18 (about 1.1×10^7 , not optimal in the first round). 2) Regardless of the scale of the learning rate, the transformed features are always normalized, which facilitates training with a relatively large learning rate. In contrast, in traditional FL, only an appropriate learning rate leads to good performance.

C. Privacy Guarantee

In traditional FL, the original data are kept locally and are not sent to the server, thereby ensuring data privacy. In LoLaFL, although the original data remain local, the transmitted parameters are related to features that are transformed from the original data. We will demonstrate that, for both the HM-like and CM-based schemes in LoLaFL, it is not possible to derive the features from the transmitted parameters, let alone recovering the original data. The details are as follows.

Let $\mathbf{Z}_{\ell,k}^j$ be the features belonging to class j in layer ℓ at edge device k . For the edge server, even if it can get the CMs by either using (17) as

$$\mathbf{Z}_{\ell,k}^j \mathbf{Z}_{\ell,k}^{j*} = \mathbf{Z}_{\ell,k} \mathbf{\Pi}_k^j \mathbf{Z}_{\ell,k}^* = (\mathbf{C}_\ell^j)^{-1} - (1/\alpha_k^j) \mathbf{I}$$

(for the HM-like scheme) or receiving directly (for the CM-based scheme), it cannot recover the original features $\mathbf{Z}_{\ell,k}^j$ from the CMs, and the reasoning is as follows. Denote $\mathbf{Y} \triangleq \mathbf{Z}_{\ell,k}^j \mathbf{Z}_{\ell,k}^{j*}$, as the calculated/received positive semi-definite matrix. Indeed we can find a solution \mathbf{Z}_0 for equation $\mathbf{Z}\mathbf{Z}^* = \mathbf{Y}$ which satisfies $\mathbf{Z}_0 \mathbf{Z}_0^* = \mathbf{Y}$ (e.g., by Cholesky

factorization [49]). But for any orthogonal matrix \mathbf{Q} , $\mathbf{Z}_1 = \mathbf{Z}_0 \mathbf{Q}$ is also a solution for equation $\mathbf{Z}\mathbf{Z}^* = \mathbf{Y}$ because $\mathbf{Z}_1 \mathbf{Z}_1^* = \mathbf{Z}_0 \mathbf{Q} \mathbf{Q}^* \mathbf{Z}_0^* = \mathbf{Y}$. Therefore, the solution is not unique unless other constraints are provided, which means the original features $\mathbf{Z}_{\ell,k}^j$ cannot be derived.

Still, there is one exception where original $\mathbf{Z}_{\ell,k}^j$ can be obtained exactly, i.e., the sample number of some classes in some devices is only 1. In this situation, we can obtain the original data $\mathbf{Z}_{\ell,k}^j = [\sqrt{\mathbf{Y}(1,1)}, \sqrt{\mathbf{Y}(2,2)}, \dots, \sqrt{\mathbf{Y}(d,d)}]^*$ from the received \mathbf{Y} . Here the aforementioned orthogonal matrix \mathbf{Q} degenerates into a number, namely one, hereby resulting the unique solution. However, we can safely ignore this exception, if we assume that there are no devices where there is only one sample belonging to a certain class.

For an edge device, it can only obtain the CMs of the other edge device when $K = 2$, by subtracting its own local CMs from the global CMs which are either calculated (for the HM-like scheme) or received (for the CM-based scheme). However, even in this scenario, the original features of the other device cannot be derived due to the same reasoning as for the edge server. Consequently, we conclude that both proposed schemes provide a privacy guarantee.

VI. EXPERIMENTAL RESULTS

A. Experimental Settings

- **Communication setting:** We consider a FL system comprising an edge server and $K = 10$ edge devices. The available frequency spectrum with bandwidth $B = 10$ MHz is divided into $M = K$ orthogonal subchannels. The threshold for truncated channel inversion is set as $\tau = 0.105$, which corresponds to an outage probability of about $\xi = 0.1$. Device k uploads local parameters only when $|h_k|^2 \geq \tau$, otherwise it quits parameters uploading in this round. To guarantee a high quantization resolution, we set $Q = 32$ [24].
- **Metrics:** The test accuracy and total latency are two important metrics used to compare the performance of LoLaFL and traditional FL. The former utilizes the test set to assess the model at each learning stage, indicating how well the model is trained and its ability to generalize. The specific definition of the latter metric is given by

$$T_{\text{total}} = \sum_{\ell=1}^{L'} \max_{k \in \mathcal{K}} \{T_{\text{comm},\ell,k} + T_{\text{comp},\ell,k}\}, \quad (24)$$

where L' represents a given number of communication rounds, and $T_{\text{comp},\ell,k}$ is the computation latency for

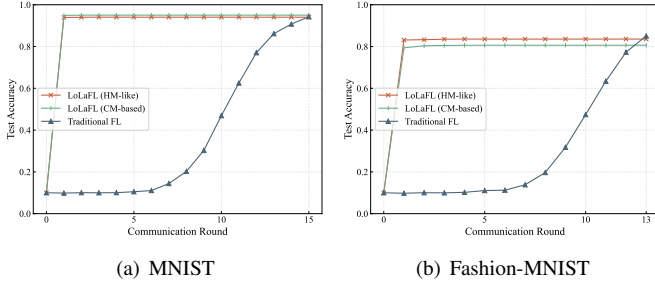


Fig. 3: Learning performance comparison between LoLaFL and traditional FL w.r.t. communication round.

device k in round ℓ . A total of 50 IID experiments are conducted with different channel realizations, to yield the average performance. Specifically, we evaluate the performance at each communication round, averaging the test accuracy and total latency up to that round.

- **LoLaFL schemes:** The hyperparameters in LoLaFL schemes are as follows: $L = 1$, $\eta = 5$, $\epsilon = 1$, $\lambda = 500$. For LoLaFL with CM-based aggregation, $\beta_0 = 0.98$.
- **Traditional FL scheme:** We implement traditional FL using ResNet-18, whose parameter number is approximately $W = 1.1 \times 10^7$ and the learning rate is set as $\eta = 0.1$ [45].
- **Real-world datasets:** Two popular datasets, MNIST and Fashion-MNIST, are utilized in the experiments. Both datasets consist of a training set containing 60,000 labeled data samples and a test set of 10,000 labeled data samples, each comprising 10 classes. The MNIST dataset consists of handwritten digits ranging from 0 to 9, while the Fashion-MNIST dataset includes common objects such as trousers and dresses. The images in both datasets are grayscale and have a size of 28×28 . Consequently, we have $d = 28 \times 28 = 784$ and $J = 10$ for both datasets. Each device is assigned $m_k = 1,200$ labeled data samples for training and the samples from different devices do not overlap. Two settings of data partitioning are considered: IID and non-IID. In the IID setting, each device randomly obtains m_k labeled data samples from the training set. For the non-IID setting, $m_k \times K$ samples are randomly selected from the training set first, which are then sorted according to their respective classes and sequentially allocated to each device. For testing, all 10,000 samples from the test set are used.

B. Learning Performance of LoLaFL

The performance of LoLaFL and traditional FL is compared in Fig. 3-4. We begin by examining the convergence characteristics of LoLaFL with HM-like and CM-based aggregations. For the MNIST dataset, the two schemes for LoLaFL exhibit nearly identical increases in test accuracy as the number of layers increases, with LoLaFL with CM-based aggregation showing a slight advantage. In contrast, for the more complex Fashion-MNIST dataset, LoLaFL with HM-like aggregation

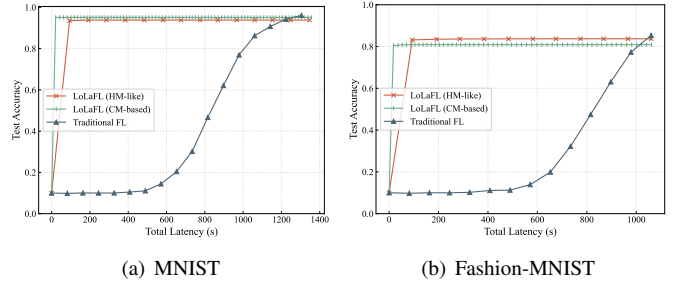


Fig. 4: Learning performance comparison between LoLaFL and traditional FL w.r.t. total latency.

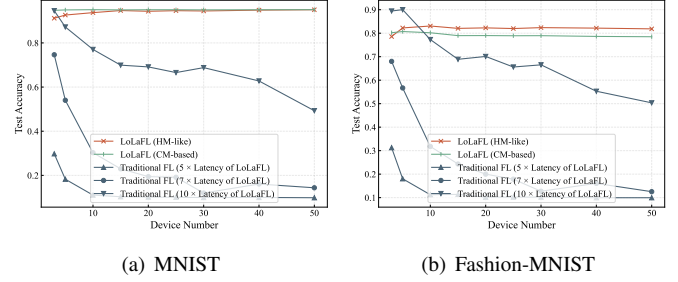


Fig. 5: Learning performance comparison between LoLaFL and traditional FL w.r.t. device number.

achieves a higher accuracy, serving as the upper bound. The CM-based scheme approaches this upper bound, but a noticeable gap remains due to information loss resulting from the low-rank approximation employed in the CM-based scheme. Another important observation is that the accuracy of the white-box schemes has achieved a high level even in the first layer, while the subsequent layers contribute to a limited increase in accuracy. This observation motivates us to transmit only the first layer in LoLaFL and justifies why we set $L = 1$ in the following experiments.

While traditional FL has the potential to outperform LoLaFL when given sufficient rounds, the required number of rounds and total latency are considerable. Generally, traditional FL needs more than 12 rounds to surpass LoLaFL. This demonstrates the advantage of LoLaFL over traditional FL: to achieve comparable accuracy, LoLaFL requires only 1/10 of the communication rounds compared to traditional FL, suppressing the communication overhead between the edge device and the edge server. When considering the total latency required for comparable accuracy, the HM-like and CM-based schemes in LoLaFL require less than 9% and 2% of the total latency associated with traditional FL.

C. Effects of Network Parameters

We investigate the effects of two important network parameters, i.e., the device number and the outage probability on LoLaFL. With the current data allocation setting, more devices mean more samples are available for training. Fig. 5 indicates that the device number does not significantly influence LoLaFL. This is because LoLaFL directly calculates the

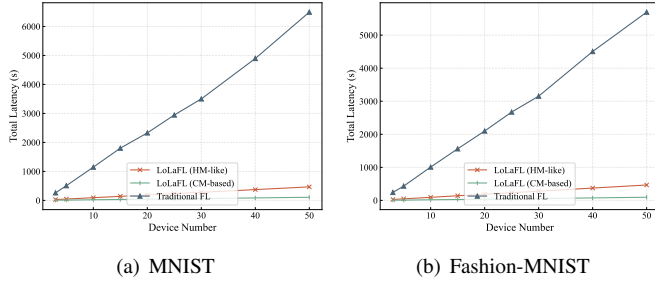


Fig. 6: Total latency comparison between LoLaFL and traditional FL w.r.t. device number constrained by specific test accuracy. (a) Approximately 94% test accuracy; (b) Approximately 79% test accuracy.

NN parameters from the features, which captures the inherent structures of the data and features. Thus, even a portion of the training set is sufficient to ensure satisfactory accuracy. In contrast, as the device number increases, the convergence speed of traditional FL is heavily affected, resulting in poor performance even when the total latency is 10 times greater than that of LoLaFL. Although the available training samples increase, in traditional FL, local training during each communication round causes deviations of local models from the global model, and this phenomenon is exacerbated by the increasing number of devices, resulting in the performance degradation of traditional FL. Fig. 6 illustrates the total latency required to achieve satisfactory test accuracy across different schemes, where it is ensured that the test accuracy of traditional FL does not exceed that of LoLaFL at any number of devices. Although the total latency for all three schemes generally increases linearly with device number, the rate of change for traditional FL is significantly steeper than that of LoLaFL. Consequently, traditional FL requires greater latency to achieve performance comparable to that of LoLaFL. This suggests that traditional FL is not suitable for scenarios with a large number of devices.

Fig. 7 illustrates the impacts of outage probability on different schemes, demonstrating how different schemes perform under different channel conditions. The curves indicate that the performance of LoLaFL degrades when the outage probability exceeds approximately 0.6. This observation aligns with prior analysis: outages lead to a reduction in available samples for training, yet only a portion of the training samples are sufficient for accurately constructing the NN parameters for LoLaFL. In contrast, traditional FL is affected even when the outage probability is below 0.1. This is because, in traditional FL, device outages can result in biased gradient estimations, leading to inefficient model training, which slows convergence and degrades performance. As shown in the figure, LoLaFL outperforms traditional FL in almost all outage probabilities, achieving this while utilizing only 1/10 of the total latency of traditional FL. The observed tendency for higher outage probability correlating with increased test accuracy for traditional FL once the outage probability exceeds 0.5 may be attributed to the fact that outages function similarly to dropout in neural

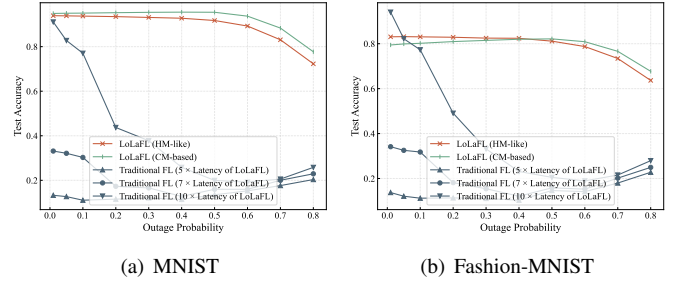


Fig. 7: Learning performance comparison between LoLaFL and traditional FL w.r.t. outage probability.

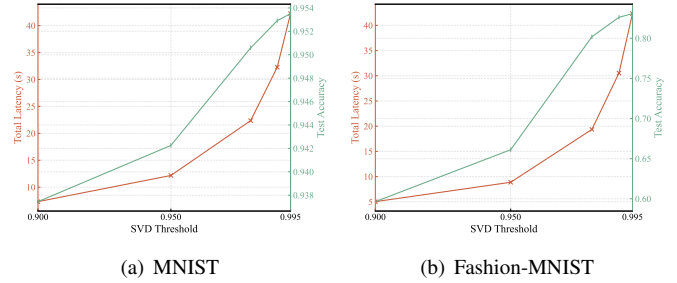


Fig. 8: The effects of SVD threshold on LoLaFL with CM-based aggregation.

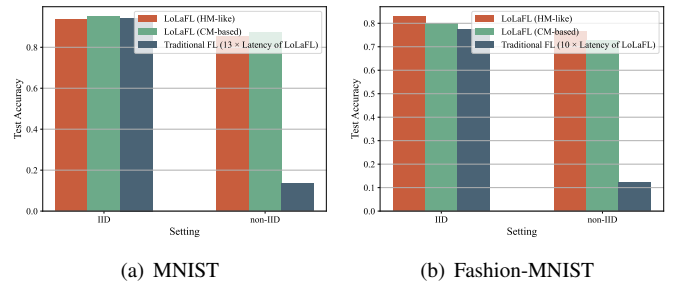


Fig. 9: Learning performance comparison between LoLaFL and traditional FL on IID and non-IID settings.

network training, thereby reducing overfitting [37].

D. Compression of Covariance Matrices

We investigate how the SVD threshold influences the total latency and test accuracy for LoLaFL with CM-based aggregation, as shown in Fig. 8. Theoretically, a higher SVD threshold permits the transmission of more singular vectors and values, which results in two key effects: 1) an increase in communication overhead, thereby increasing the total latency, and 2) a reduction in information loss within the reconstructed parameters, leading to improved learning performance. The curves presented in Fig. 8 agree with these expectations. This justifies our choice of setting the threshold to 0.98 in our experiments, for the sake of achieving the best trade-off between accuracy and latency.

E. IID and Non-IID

We investigate the influence of the non-IID setting on LoLaFL and traditional FL, as shown in Fig. 9. The non-IID setting has a minor influence on LoLaFL, while it significantly affects traditional FL, demonstrating the substantial advantage of LoLaFL when dealing with non-IID data. For LoLaFL, the NN parameters are calculated from features directly, which means that the results remain consistent regardless of how data are distributed across different devices, assuming the distortion induced by the channel is ignored. In contrast, for traditional FL, the heterogeneous data across different devices exacerbate the deviation of local models from the global model, leading to slower convergence and degraded performance.

VII. CONCLUDING REMARKS

In this paper, we have proposed the use of the state-of-the-art white-box approach to develop the novel LoLaFL framework accompanied by two novel nonlinear aggregation schemes. Compared with traditional FL, LoLaFL with HM-like and CM-based aggregation demonstrate tenfold and hundredfold reductions in latency, respectively, while maintaining comparable accuracies. This drastic performance improvement mainly results from the novel FL framework with forward-only propagation to achieve rapid convergence. LoLaFL is particularly beneficial when the data dimensionality and the class number are small but low latency is required, especially in scenarios when computation and communication resources are severely limited and the data are non-IID.

Several directions for further research are worth exploring to overcome the limitation of LoLaFL. Firstly, the development of an improved coding theory to characterize the volume of the feature space and employing advanced optimization approaches could enhance the learning performance. Secondly, focusing on achieving higher compression rates, particularly in relation to exploiting the sparsity of the features, can further reduce the communication latency. Lastly, some dimensionality reduction techniques can be applied to the original data before they are utilized in LoLaFL. This approach can significantly reduce both communication latency and computation latency.

APPENDIX

A. Proof of Lemma 1

For any permutation matrix \mathbf{P} , we have $\mathbf{Z}_\ell \mathbf{P} (\mathbf{Z}_\ell \mathbf{P})^* = \mathbf{Z}_\ell \mathbf{P} \mathbf{P}^* \mathbf{Z}_\ell^* \stackrel{(a)}{=} \mathbf{Z}_\ell \mathbf{Z}_\ell^*$, where (a) is due to the property of the permutation matrix [49]. This suggests that the sample order of \mathbf{Z}_ℓ does not influence the global covariance matrix. Therefore, without loss of generality, we let $\mathbf{Z}_\ell \triangleq [\mathbf{Z}_{\ell,1}, \mathbf{Z}_{\ell,2}, \dots, \mathbf{Z}_{\ell,K}]$, and thus

$$\mathbf{\Pi}^j = \begin{bmatrix} \mathbf{\Pi}_1^j & & & \\ & \mathbf{\Pi}_2^j & & \\ & & \ddots & \\ & & & \mathbf{\Pi}_K^j \end{bmatrix}. \quad (25)$$

By using matrix partition and the corresponding multiplication law, we have (26) and (27).

$$\begin{aligned} \mathbf{Z}_\ell \mathbf{Z}_\ell^* &= [\mathbf{Z}_{\ell,1}, \mathbf{Z}_{\ell,2}, \dots, \mathbf{Z}_{\ell,K}] [\mathbf{Z}_{\ell,1}, \mathbf{Z}_{\ell,2}, \dots, \mathbf{Z}_{\ell,K}]^* \\ &= \sum_{k=1}^K \mathbf{Z}_{\ell,k} \mathbf{Z}_{\ell,k}^* \end{aligned} \quad (26)$$

$$\begin{aligned} \mathbf{Z}_\ell \mathbf{\Pi}^j \mathbf{Z}_\ell^* &= [\mathbf{Z}_{\ell,1}, \mathbf{Z}_{\ell,2}, \dots, \mathbf{Z}_{\ell,K}] \begin{bmatrix} \mathbf{\Pi}_1^j & & & \\ & \mathbf{\Pi}_2^j & & \\ & & \ddots & \\ & & & \mathbf{\Pi}_K^j \end{bmatrix} \begin{bmatrix} \mathbf{Z}_{\ell,1}^* \\ \mathbf{Z}_{\ell,2}^* \\ \vdots \\ \mathbf{Z}_{\ell,K}^* \end{bmatrix} \\ &= \sum_{k=1}^K \mathbf{Z}_{\ell,k} \mathbf{\Pi}_k^j \mathbf{Z}_{\ell,k}^* \end{aligned} \quad (27)$$

Therefore, the proof is completed. \square

B. Proof of Proposition 1

By transforming (16) and (17), we have (28) and (29).

$$\mathbf{Z}_{\ell,k} \mathbf{Z}_{\ell,k}^* = (\mathbf{E}_{\ell,k})^{-1} - (1/\alpha_k) \mathbf{I} \quad (28)$$

$$\mathbf{Z}_{\ell,k} \mathbf{\Pi}_k^j \mathbf{Z}_{\ell,k}^* = (\mathbf{C}_{\ell,k})^{-1} - (1/\alpha_k^j) \mathbf{I} \quad (29)$$

Therefore, we have

$$\begin{aligned} \bar{\mathbf{E}}_\ell &= \alpha (\mathbf{I} + \alpha \mathbf{Z}_\ell \mathbf{Z}_\ell^*)^{-1} \\ &\stackrel{(a)}{=} \alpha \left(\mathbf{I} + \alpha \sum_{k=1}^K \mathbf{Z}_{\ell,k} \mathbf{Z}_{\ell,k}^* \right)^{-1} \\ &\stackrel{(b)}{=} \alpha \left(\mathbf{I} + \alpha \sum_{k=1}^K \left((\mathbf{E}_{\ell,k})^{-1} - (1/\alpha_k) \mathbf{I} \right) \right)^{-1} \\ &= \alpha \left(\left(1 - \alpha \sum_{k=1}^K 1/\alpha_k \right) \mathbf{I} + \alpha \sum_{k=1}^K (\mathbf{E}_{\ell,k})^{-1} \right)^{-1} \\ &\stackrel{(c)}{=} \alpha \left(\alpha \sum_{k=1}^K (\mathbf{E}_{\ell,k})^{-1} \right)^{-1} = \left(\sum_{k=1}^K (\mathbf{E}_{\ell,k})^{-1} \right)^{-1}, \end{aligned} \quad (30)$$

where equality (a) holds because of Lemma 1, (b) holds because of (28), and (c) holds because $\sum_{k=1}^K 1/\alpha_k = \sum_{k=1}^K m_k \epsilon^2 / d = m \epsilon^2 / d = 1/\alpha$. Also, we have

$$\begin{aligned} \bar{\mathbf{C}}_\ell^j &= \alpha^j (\mathbf{I} + \alpha^j \mathbf{Z}_\ell \mathbf{\Pi}^j \mathbf{Z}_\ell^*)^{-1} \\ &\stackrel{(a)}{=} \alpha^j \left(\mathbf{I} + \alpha^j \sum_{k=1}^K \mathbf{Z}_{\ell,k} \mathbf{\Pi}_k^j \mathbf{Z}_{\ell,k}^* \right)^{-1} \\ &\stackrel{(b)}{=} \alpha^j \left(\mathbf{I} + \alpha^j \sum_{k=1}^K \left((\mathbf{C}_{\ell,k}^j)^{-1} - (1/\alpha_k^j) \mathbf{I} \right) \right)^{-1} \\ &= \alpha^j \left(\left(1 - \alpha^j \sum_{k=1}^K 1/\alpha_k^j \right) \mathbf{I} + \alpha^j \sum_{k=1}^K (\mathbf{C}_{\ell,k}^j)^{-1} \right)^{-1} \\ &\stackrel{(c)}{=} \alpha^j \left(\alpha^j \sum_{k=1}^K (\mathbf{C}_{\ell,k}^j)^{-1} \right)^{-1} = \left(\sum_{k=1}^K (\mathbf{C}_{\ell,k}^j)^{-1} \right)^{-1}, \end{aligned} \quad (31)$$

where equality (a) holds because of Lemma 1, (b) holds because of (29), and (c) holds because $\sum_{k=1}^K 1/\alpha_k^j = \sum_{k=1}^K \text{tr}(\mathbf{\Pi}_k^j)\epsilon^2/d = \text{tr}(\mathbf{\Pi}^j)\epsilon^2/d = 1/\alpha^j$. \square

REFERENCES

- [1] K. B. Letaief, W. Chen, Y. Shi, J. Zhang, and Y.-J. A. Zhang, "The roadmap to 6g: Ai empowered wireless networks," *IEEE Commun. Mag.*, vol. 57, no. 8, pp. 84–90, 2019.
- [2] W. Saad, M. Bennis, and M. Chen, "A vision of 6g wireless systems: Applications, trends, technologies, and open research problems," *IEEE Netw.*, vol. 34, no. 3, pp. 134–142, 2019.
- [3] G. Zhu, D. Liu, Y. Du, C. You, J. Zhang, and K. Huang, "Toward an intelligent edge: Wireless communication meets machine learning," *IEEE Commun. Mag.*, vol. 58, no. 1, pp. 19–25, 2020.
- [4] Z. Wang, A. E. Kalør, Y. Zhou, P. Popovski, and K. Huang, "Ultra-low-latency edge inference for distributed sensing," *arXiv preprint arXiv:2407.13360*, 2024.
- [5] B. McMahan, E. Moore, D. Ramage, S. Hampson, and B. A. y Arcas, "Communication-efficient learning of deep networks from decentralized data," in *Artificial Intelligence and Statist.*, pp. 1273–1282, PMLR, 2017.
- [6] L. U. Khan, W. Saad, Z. Han, E. Hossain, and C. S. Hong, "Federated learning for internet of things: Recent advances, taxonomy, and open challenges," *IEEE Commun. Surveys Tuts.*, vol. 23, no. 3, pp. 1759–1799, 2021.
- [7] Z. Li, Z. Lin, J. Shao, Y. Mao, and J. Zhang, "Fedcir: Client-invariant representation learning for federated non-iid features," *IEEE Trans. Mobile Comput.*, 2024.
- [8] Z. Lin, G. Zhu, Y. Deng, X. Chen, Y. Gao, K. Huang, and Y. Fang, "Efficient parallel split learning over resource-constrained wireless edge networks," *IEEE Trans. Mobile Comput.*, 2024.
- [9] R. Singh, A. Kaushik, W. Shin, M. Di Renzo, V. Sciancalepore, D. Lee, H. Sasaki, A. Shojaeifard, and O. A. Dobre, "Towards 6g evolution: Three enhancements, three innovations, and three major challenges," *arXiv:2402.10781*. [Online] <https://arxiv.org/abs/2402.10781>, 2024.
- [10] Z. Ma, M. Xiao, Y. Xiao, Z. Pang, H. V. Poor, and B. Vucetic, "High-reliability and low-latency wireless communication for internet of things: Challenges, fundamentals, and enabling technologies," *IEEE Internet Things J.*, vol. 6, no. 5, pp. 7946–7970, 2019.
- [11] X. Deng, J. Li, C. Ma, K. Wei, L. Shi, M. Ding, and W. Chen, "Low-latency federated learning with dnn partition in distributed industrial iot networks," *IEEE J. Sel. Areas Commun.*, vol. 41, no. 3, pp. 755–775, 2022.
- [12] W. Y. B. Lim, N. C. Luong, D. T. Hoang, Y. Jiao, Y.-C. Liang, Q. Yang, D. Niyato, and C. Miao, "Federated learning in mobile edge networks: A comprehensive survey," *IEEE Commun. Surveys Tuts.*, vol. 22, no. 3, pp. 2031–2063, 2020.
- [13] M. Bennis, M. Debbah, and H. V. Poor, "Ultrareliable and low-latency wireless communication: Tail, risk, and scale," *Proceedings of the IEEE*, vol. 106, no. 10, pp. 1834–1853, 2018.
- [14] P. Yang, L. Kong, and G. Chen, "Spectrum sharing for 5g/6g urllc: Research frontiers and standards," *IEEE Commun. Stand. Mag.*, vol. 5, no. 2, pp. 120–125, 2021.
- [15] Q. Zeng, Y. Du, and K. Huang, "Wirelessly powered federated edge learning: Optimal tradeoffs between convergence and power transfer," *IEEE Trans. Wireless Commun.*, vol. 21, no. 1, pp. 680–695, 2021.
- [16] Z. Yang, M. Chen, W. Saad, C. S. Hong, and M. Shikh-Bahaei, "Energy efficient federated learning over wireless communication networks," *IEEE Trans. Wireless Commun.*, vol. 20, no. 3, pp. 1935–1949, 2020.
- [17] H. Zhang, M. Tao, Y. Shi, X. Bi, and K. B. Letaief, "Federated multi-task learning with non-stationary and heterogeneous data in wireless networks," *IEEE Trans. Wireless Commun.*, 2023.
- [18] D. Wen, M. Bennis, and K. Huang, "Joint parameter-and-bandwidth allocation for improving the efficiency of partitioned edge learning," *IEEE Trans. Wireless Commun.*, vol. 19, no. 12, pp. 8272–8286, 2020.
- [19] Z. Wang, K. Huang, and Y. C. Eldar, "Spectrum breathing: Protecting over-the-air federated learning against interference," *IEEE Trans. Wireless Commun.*, 2024.
- [20] L. Zeng, D. Wen, G. Zhu, C. You, Q. Chen, and Y. Shi, "Federated learning with energy harvesting devices," *IEEE Trans. Green Commun. Netw.*, 2023.
- [21] M. Chen, Z. Yang, W. Saad, C. Yin, H. V. Poor, and S. Cui, "A joint learning and communications framework for federated learning over wireless networks," *IEEE Trans. Wireless Commun.*, vol. 20, no. 1, pp. 269–283, 2020.
- [22] G. Zhu, Y. Wang, and K. Huang, "Broadband analog aggregation for low-latency federated edge learning," *IEEE Trans. Wireless Commun.*, vol. 19, no. 1, pp. 491–506, 2019.
- [23] K. Yang, T. Jiang, Y. Shi, and Z. Ding, "Federated learning via over-the-air computation," *IEEE Trans. Wireless Commun.*, vol. 19, no. 3, pp. 2022–2035, 2020.
- [24] Z. Liu, Q. Lan, A. E. Kalør, P. Popovski, and K. Huang, "Over-the-air multi-view pooling for distributed sensing," *IEEE Trans. Wireless Commun.*, 2023.
- [25] Z. Chen, X. Y. Zhang, D. K. So, K.-K. Wong, C.-B. Chae, and J. Wang, "Federated learning driven sparse code multiple access in v2x communications," *IEEE Netw.*, 2024.
- [26] W. Xia, W. Wen, K.-K. Wong, T. Q. Quek, J. Zhang, and H. Zhu, "Federated-learning-based client scheduling for low-latency wireless communications," *IEEE Wireless Commun.*, vol. 28, no. 2, pp. 32–38, 2021.
- [27] Z. Lin, G. Qu, X. Chen, and K. Huang, "Split learning in 6g edge networks," *IEEE Wireless Commun.*, 2024.
- [28] Z. Lin, G. Qu, W. Wei, X. Chen, and K. K. Leung, "Adaptfsf: Adaptive split federated learning in resource-constrained edge networks," *arXiv preprint arXiv:2403.13101*, 2024.
- [29] W. Ni, H. Ao, H. Tian, Y. C. Eldar, and D. Niyato, "Fedsl: Federated split learning for collaborative healthcare analytics on resource-constrained wearable iomt devices," *IEEE Internet Things J.*, 2024.
- [30] M. Zhang, Y. Li, D. Liu, R. Jin, G. Zhu, C. Zhong, and T. Q. Quek, "Joint compression and deadline optimization for wireless federated learning," *IEEE Trans. Mobile Comput.*, 2023.
- [31] G. Zhu, Y. Du, D. Gündüz, and K. Huang, "One-bit over-the-air aggregation for communication-efficient federated edge learning: Design and convergence analysis," *IEEE Trans. Wireless Commun.*, vol. 20, no. 3, pp. 2120–2135, 2020.
- [32] M. Xu, D. T. Hoang, J. Kang, D. Niyato, Q. Yan, and D. I. Kim, "Secure and reliable transfer learning framework for 6g-enabled internet of vehicles," *IEEE Wireless Commun.*, vol. 29, no. 4, pp. 132–139, 2022.
- [33] Y. LeCun, L. Bottou, Y. Bengio, and P. Haffner, "Gradient-based learning applied to document recognition," *Proc. IEEE*, vol. 86, no. 11, pp. 2278–2324, 1998.
- [34] D. E. Rumelhart, G. E. Hinton, and R. J. Williams, "Learning representations by back-propagating errors," *nature*, vol. 323, no. 6088, pp. 533–536, 1986.
- [35] K. He, X. Zhang, S. Ren, and J. Sun, "Delving deep into rectifiers: Surpassing human-level performance on imagenet classification," in *Proc. IEEE Int. Conf. Comput. Vis.*, pp. 1026–1034, 2015.
- [36] B. Xu, N. Wang, T. Chen, and M. Li, "Empirical evaluation of rectified activations in convolutional network," *arXiv preprint arXiv:1505.00853*, 2015.
- [37] N. Srivastava, G. Hinton, A. Krizhevsky, I. Sutskever, and R. Salakhutdinov, "Dropout: a simple way to prevent neural networks from overfitting," *J. Mach. Learn. Res.*, vol. 15, no. 1, pp. 1929–1958, 2014.
- [38] G. Montavon, W. Samek, and K.-R. Müller, "Methods for interpreting and understanding deep neural networks," *Digital signal processing*, vol. 73, pp. 1–15, 2018.
- [39] Y. Ma, D. Tsao, and H.-Y. Shum, "On the principles of parsimony and self-consistency for the emergence of intelligence," *Front. Inf. Technol. Electron. Eng.*, vol. 23, no. 9, pp. 1298–1323, 2022.
- [40] K. H. R. Chan, Y. Yu, C. You, H. Qi, J. Wright, and Y. Ma, "Redunet: A white-box deep network from the principle of maximizing rate reduction," *J. Mach. Learn. Res.*, vol. 23, no. 1, pp. 4907–5009, 2022.
- [41] Y. Yu, K. H. R. Chan, C. You, C. Song, and Y. Ma, "Learning diverse and discriminative representations via the principle of maximal coding rate reduction," *Proc. Adv. Neural Inf. Process. Syst. (NeurIPS)*, vol. 33, pp. 9422–9434, 2020.
- [42] C. Cai, X. Yuan, and Y.-J. A. Zhang, "Multi-device task-oriented communication via maximal coding rate reduction," *IEEE Trans. Wireless Commun.*, 2024.
- [43] Y. Ma, H. Derksen, W. Hong, and J. Wright, "Segmentation of multivariate mixed data via lossy data coding and compression," *IEEE Trans. Pattern Anal. Mach. Intell.*, vol. 29, no. 9, pp. 1546–1562, 2007.
- [44] T. M. Cover, *Elements of information theory*. John Wiley & Sons, 1999.

- [45] K. He, X. Zhang, S. Ren, and J. Sun, "Deep residual learning for image recognition," in *Proc. IEEE Conf. Comput. Vis. Pattern Recognit.*, pp. 770–778, 2016.
- [46] I. Goodfellow, Y. Bengio, and A. Courville, *Deep learning*. MIT press, 2016.
- [47] A. Goldsmith, *Wireless communications*. Cambridge university press, 2005.
- [48] M. Abramowitz and I. A. Stegun, *Handbook of mathematical functions with formulas, graphs, and mathematical tables*, vol. 55. US Government printing office, 1968.
- [49] T. K. Moon and W. C. Stirling, "Mathematical methods and algorithms for signal processing," 2000.
- [50] G. H. Golub and C. F. Van Loan, *Matrix computations*. JHU press, 2013.
- [51] Y. LeCun, Y. Bengio, and G. Hinton, "Deep learning," *nature*, vol. 521, no. 7553, pp. 436–444, 2015.